ON THE DISTORTION OF YIELD SURFACE UNDER COMPLEX LOADING PATHS IN SHEET METAL FORMING

Z.M.Yue[1, 2]*, H. Badreddine[1], K. Saanouni[1], E.S.Perdahcioglu[3], C. Soyarslan[4], A. E. Tekkaya[2], A.H. van den Boogaard[3]

[1]ICD-LASMIS, University of Technology of Troyes / France
[2] Institute of Forming Technology and Lightweight Construction, TU Dortmund/Germany
[3] Group of Applied Mechanics, Faculty of Engineering Technology, University of Twente, P. O. Box 217, 7500 AE Enschede, Netherlands
[4]Institute of Continuum and Material Mechanics, TU Hamburg-Harburg/Germany

ABSTRACT: A novel constitutive model is proposed in which a fully coupled approach combining ductile damage, mixed nonlinear hardening and anisotropic plasticity is enhanced with the introduction of the distortion of the yield surface. The aim is to extend the capability of the model to investigate the metal sheet behavior under complex loading paths. Following the original idea of François [1], which introduced the yield surface distortion through the kinematic hardening, a new developed distorted deviatoric stress $\underline{S}_d$ is used instead of the usual deviator stress $\underline{S}$. This leads to obtaining an 'egg-shaped' yield surface as the kinematic hardening evolves. The novelty of the proposed model is the proposal of three distortion parameters which separately control the distortional ratio and the cross size of subsequent yield surfaces. This model is implemented into ABAQUS/Explicit FE code through the VUMAT user-defined subroutine. The calibration of the yield surface distortion and its effect on subsequent deformation process, are studied using tension-shear loading path. The applicability of the new model is illustrated by the simulation of the experimental results obtained with the TWENTE BIAXIAL TESTER (TBT), which can test material forming behavior under various complex loading paths.

KEYWORDS: Mixed hardening, Ductile damage, Yield surface distortion, Biaxial loading, Numerical simulation.

1 INTRODUCTION

In sheet metal forming process, it is well known that the deformation is accompanied by various kinds of initial and induced anisotropies. In order to accurately describe material behaviour in numerical simulation of metal forming processes, a comprehensive understanding of the initiation and evolution of these material anisotropies is required. Lots of works have been done on the modelling of initial anisotropies, like the quadratic Hill-type yield function with orthotropic symmetry [2-4] and non-quadratic Hosford-type yield function [5]. All these criteria introduce appropriate linear transformations of stress tensor with some multiple fitting parameters. They assume that the initial anisotropy is due to the texture induced during the rolling process of the sheet. For induced anisotropies, a number of publications proposed approaches for modelling the distortion of the yield surfaces [1, 6-9]. François [1] proposed a yield criterion using the same norm as in the classical von Mises based criteria and a distortional stress replacing the common stress deviator in this criterion. On the other hand, Feigenbaum and Dafalias [7, 10] introduced a thermodynamically-consistent framework of isotropic, kinematic and directional distortional hardening under small strains. Recently, Barlat et al. [8, 11] proposed a new approach describing the material behaviour under multiple or continuous strain path. In his model, a homogeneous anisotropic yield function which combines a stable, isotropic hardening and distortional hardening by incorporating latent hardening effects is proposed which can well capture the material behaviour during cross-loading.

For damage prediction, it is also a big issue to well understand the evolution of the subsequent yield surfaces under proportional and non-proportional loading paths for which the failure is very sensitive to the small changes of the yield surface due to the strong interactions between hardening and damage. In this paper, an enhanced fully coupled ductile

* Corresponding author: 12 Rue Marie Curie CS 42060, 10004 Troyes Cedex, France; Tel.: +33 3 25 71 80 23; Fax: +33 3 25 71 56 75 ; E-mail: zhenming.yue@utt.fr

damage model is proposed, which considers a general initial anisotropic yield function with mixed nonlinear kinematic and isotropic hardening. The distortion of the yield surface due to the plastic strain with hardening is also accounted in a new developed form. In order to test the capability of the proposed model, the forming behavior of sheet metal AL7020 is investigated using monotonic and orthogonal loading paths. The orthogonal loading paths are applied the TBT experimental device [12] and includes tension-shear and shear-tension loading sequences. The elastoplastic and damage parameters of the model are first determined using simple uniaxial tensile tests, notched tensile tests, in-plane torsion tests and simple shear tests. Then, the combined loading paths are applied using TBT device to investigate the evolution of the yield surfaces with the help of optical measurement system. For AL7020 one test is conducted until the final fracture in order to investigate the damage occurrence and the influence of the directional hardening in the damage growth.

2 Material model

Based on continuum damage mechanics within a thermodynamics framework, the elastoplastic constitutive equations fully coupled with the isotropic ductile damage are proposed, in which the yield surface distortion is introduced through the kinematic hardening. The following couples of state variables are used: $(\underline{\varepsilon}^e, \underline{\sigma})$ representing the elastoplastic flow; $(\underline{\alpha}, \underline{X})$ representing the kinematic hardening depicting the translation of the yield surface; (r, R) representing the isotropic hardening depicting the size (radius) of the yield surface; (d, Y) representing the isotropic ductile damage. The detailed formulation of this type of constitutive equations can be found in ([13], [14]). We limit ourselves here to give the final form of the constitutive equations in which the kinematic hardening induced distortion is introduced:

- The state relations are:

$$\underline{\sigma} = 2\mu_e\left[(1-d)\left\langle \underline{e}_e \right\rangle_+ + (1-hd)\left\langle \underline{e}_e \right\rangle_-\right] + \lambda_e\left[(1-d)\left\langle tr(\underline{\varepsilon}_e)\right\rangle - (1-hd)\left\langle -tr(\underline{\varepsilon}_e)\right\rangle\right]\underline{1} \quad (1)$$

$$\underline{X} = (1-d)\frac{2}{3}C\underline{\alpha} \quad (2)$$

$$R = (1-d^\gamma)Qr \quad (3)$$

$$Y = Y_e + Y_\alpha + Y_r \quad (4)$$

$$Y_e = 2\mu_e\left[\left\langle \underline{e}_e \right\rangle_+ : \left\langle \underline{e}_e \right\rangle_+ + h\left\langle \underline{e}_e \right\rangle_- : \left\langle \underline{e}_e \right\rangle_-\right] + k_e\left[\left\langle tr(\underline{\varepsilon}_e)\right\rangle^2 + h\left\langle -tr(\underline{\varepsilon}_e)\right\rangle^2\right] \quad (5)$$

$$Y_\alpha = \frac{1}{3}C\underline{\alpha} : \underline{\alpha} \quad (6)$$

$$Y_r = \frac{1}{2}\gamma d^{\gamma-1}Qr^2 \quad (7)$$

where μ_e and λ_e are the Lame's constants and k_e is the compressibility modulus, while the parameters C and Q are the kinematic and the isotropic hardening moduli respectively. γ is a parameter governing the effect of the ductile damage on the isotropic hardening compared to the kinematic hardening and elastic behavior. The notation $\langle . \rangle$ indicates Macaulay brackets, i.e. $\langle x \rangle = x$ if $x \geq 0$ and $\langle x \rangle = 0$ if $\langle x \rangle \leq 0$. $\underline{1}$ denotes the unit second-rank tensor. In order to account for the microcracks closure h effect on the damage growth, the Cauchy stress tensor $\underline{\sigma}$ is spectrally decomposed into positive part $\langle \underline{\sigma} \rangle_+$ and negative part $\langle \underline{\sigma} \rangle_-$ according to $\underline{\sigma} = \langle \underline{\sigma} \rangle_+ + \langle \underline{\sigma} \rangle_-$ where $\langle \underline{\sigma} \rangle_+ = \sum_{i=1}^{3} \langle \sigma_i \rangle \vec{e}_i \otimes \vec{e}_i$ and where σ_i is the i[th] eigenvalue of the stress tensor $\underline{\sigma}$ and $\vec{e}_i$ its associated eigenvector. $\underline{e}_e = \underline{\varepsilon}_e - (1/3)\, trace(\underline{\varepsilon}_e)\underline{1}$ is the deviatoric part of the small elastic strain tensor.

- The evolution equations are:

$$f(\underline{\sigma}, \underline{X}, R; d) = \frac{\|\underline{S}_d - \underline{X}\|_H}{\sqrt{1-d}} - \frac{R}{\sqrt{1-d^\gamma}} - \sigma_y \leq 0 \quad (8)$$

$$\underline{\dot{\varepsilon}}^p = \dot{\lambda}\frac{\partial f}{\partial \underline{\sigma}} = \dot{\lambda}\underline{n}^p \quad (12)$$

$$\underline{n}^p = \frac{\underline{n}_d}{\sqrt{1-d}} : \left[\underline{\underline{1}}^{dev} + \frac{\underline{X} \otimes \underline{S}_0}{X_{I1}^p(R/\sqrt{1-d} + \sigma_y)} - \frac{\|\underline{X}\|_M}{X_{I2}}(\underline{\underline{1}}^{dev})\right] \quad (13)$$

$$\dot{\underline{\alpha}} = \dot{\lambda}\left(\frac{\tilde{\underline{n}}^x}{\sqrt{1-d}} - a\underline{\alpha}\right) \quad (14)$$

$$\tilde{\underline{n}}^x = \underline{n}_d - \frac{(\underline{S}_0 : \underline{S}_0)\underline{n}_d}{2X_{I1}^p(R/\sqrt{1-d} + \sigma_y)} + \frac{1}{X_{I2}}\left(\frac{3\underline{X} \otimes \underline{S}_0}{2\|\underline{X}\|_M}\right) : \underline{n}_d \quad (15)$$

$$\dot{r} = \dot{\lambda}\left(\frac{\tilde{n}^i}{\sqrt{1-d^\gamma}} - br\right) \quad (16)$$

$$\tilde{n}^i = \frac{(\underline{S}_0 : \underline{S}_0) \cdot (\underline{n}_d : \underline{X})}{2X_{I1}^p(\sqrt{1-d}R + (1-d)\sigma_y)^2} + 1 \quad (17)$$

$$\underline{n}_d = \frac{(\underline{S}_d - \underline{X}) : \underline{\underline{H}}}{\|\underline{S}_d - \underline{X}\|_H} \quad (18)$$

$$\dot{d} = \frac{\dot{\lambda}}{(1-d)^\beta}\left(\frac{\langle Y - Y_0 \rangle}{S}\right)^s \quad (19)$$

where a and b characterize the non-linearity of the kinematic and isotropic hardening respectively and S, s, β and Y_0 are material parameters which define the ductile damage evolution. The initial size of the yield surface is defined by σ_y or the initial yield stress.

The quadratic Hill-type equivalent stress $\|\underline{S}_d - \underline{X}\|_H = \sqrt{(\underline{S}_d - \underline{X}) : \underline{\underline{H}} : (\underline{S}_d - \underline{X})}$ is characterized by

an anisotropic operator $\underline{\underline{H}}$ having six anisotropic parameters *F, G, H, L, M* and *N*. Clearly, in this model, the "distorted stress" $\underline{S}_d$ plays an important role in the description of the yield surface distortion. The deviatoric stress $\underline{S}_d$ is different from the one proposed in Francois model [1]. A new term is introduced to control the cross size (perpendicular to loading direction) of subsequent yield surface:

$$\underline{S}_d = \underline{S} + \frac{\underline{S}_0 : \underline{S}_0}{2X_{I1}^c(R/\sqrt{1-d}+\sigma_y)}\underline{X} - \frac{\|\underline{X}\|_M}{X_{I2}}\underline{S}_0 \quad (10)$$

$$\underline{S}_x = \frac{3\underline{S}:\underline{X}}{2\|\underline{X}\|_M^2}\cdot\underline{X} \quad \text{and} \quad \underline{S}_0 = \underline{S} - \underline{S}_x \quad (11)$$

where $\|\underline{X}\|_M = \sqrt{3/2\underline{X}:\underline{X}}$ is a norm of $\underline{X}$. In this model, $\underline{S}$ is decomposed into its part $\underline{S}_X$ collinear to $\underline{X}$ and its orthogonal part $\underline{S}_o$. X_{I1} is the same as set in Francois model, used to help adjusting the distortion ratio of the subsequent yield surfaces. Two material constants X_{I1}^c and X_{I1}^p are used instead of X_{I1} in François's model. A new parameter X_{I2} was introduced into $\underline{S}_d$ to control the cross size of subsequent yield surface in the orthogonal direction of loading path.

Finally, the plastic multiplier $\dot{\lambda}$ can be determined from the consistency condition $\dot{f}^p = 0$ if $f^p = 0$, however it will be kept as the main unknown at each integration point of each finite element which will be determined from the FE calculation. This model is implemented into ABAQUS/Explicit© finite element code through the VUMAT user routine.

3 Results and discussion

The objective of this research was to investigate the behavior of 1.5 mm thickness AL7020 sheet metal. According to the convention of material property calibration, the isotropic hardening is inspected via the monotonic loading. The kinematic hardening is examined using large-amplitude, cyclic simple shear loading. The so-called distortional hardening is characterized using sequences of orthogonal strain paths. Ductile damage can be calibrated in large range of stress states. Here, in order to specify each material parameters used in the proposed model, the experimental process was separated into two steps:

- Simple loading paths: uniaxial tensile tests, notched tensile tests, in-plane torsion tests, simple shear tests (more details in [15]).
- Combined sequences loading paths using TBT device to specify and study distortional parameters X_{I1} and X_{I2}, which can affect the subsequent yield surfaces, including the yield point floating and hardening stagnation.

3.1 Identification methodology

During the calibration process, an inverse optimization program based on MATLAB is used for parameter identification. The identification methodology works based on both MATLAB code linked to ABAQUS/Explicit solver using python language script. More details concerning the identification methodology can be found in [17].

3.2 Simple loading path tests

In order to determine the elastoplastic and damage parameters, series of tests were performed to cover a large range of stress states. Detailed specimen geometries description is given in [15]. Uniaxial tensile tests allow determining the elasticity parameters and the flow hardening parameters. The torsion tests allow the separation between kinematic and isotropic hardening. For damage parameters, notched tensile tests with different radii *r* (5 mm, 10 mm, and 20 mm) and simple shear tests are performed to observe damage occurrence under different loading paths giving account for various triaxiality ratios. The overall simple tests were conducted under the displacement rate control of 0.1 mm/s to insure the quasi-static loading condition.

With the help of the identification procedure, the final determined material parameters are shown in Table.1.

Table 1: *Determined material parameters without distortion of the yield surface*

E (GPa)	ν	σ_y (MPa)	Q (MPa)	b	C (MPa)	γ
69.8	0.3	322	675	8	2260	4.0
a	F	G	H	L	M	N
75	0.631	0.634	0.366	1.5	1.5	1.4
S	s	β	Y_0	h		
4.50	1.48	3.4	0.0	0.3		

3.3 Combined loading paths tests

For the complex loading paths, the stress path change may affect the yield surface points, and the shape of the yield surface will also affect the direction of plastic flow. For damage prediction, it is also a big issue to well understand the evolution of the subsequent yield surfaces under proportional and non-proportional loading paths for which the failure is very sensitive to the small changes in the yield surface[16]. In Fig.1, the distortional parameters existing in our proposed model effect on the subsequent yield surfaces are given.

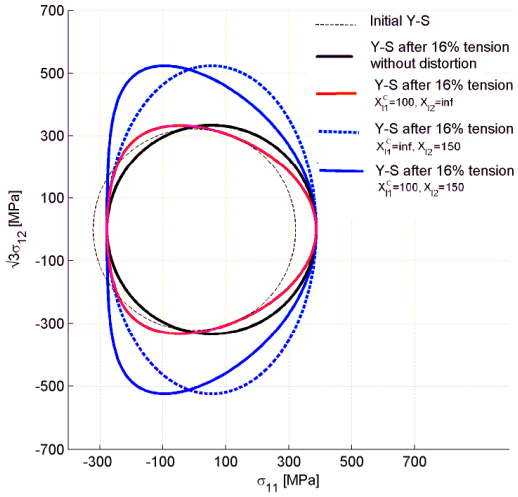

Fig. 1 *Distortional parameters effect on yield surface (Y-S) in AL7020 alloy after 16% pre-tension plastic strain.*

From Fig. 1, it is found that, with the effect of $X_{l1}^{c}=100$ the subsequent yield surfaces are distorted without surface size change, and with the effect of $X_{l2}=150$, the subsequent yield surfaces are extended in orthogonal direction without distortion. When X_{l1}^{c} and X_{l2} works together, the subsequent yield surfaces are changed to the "egg-shaped" surface with cross-size in consideration ($X_{l1}^{c}=100$, $X_{l2}=150$).

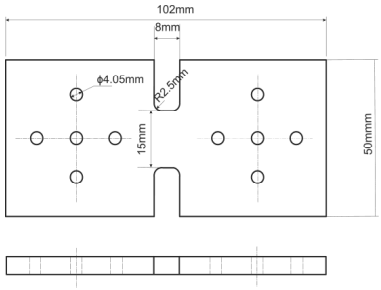

Fig. 2 *Geometry of the specimen*

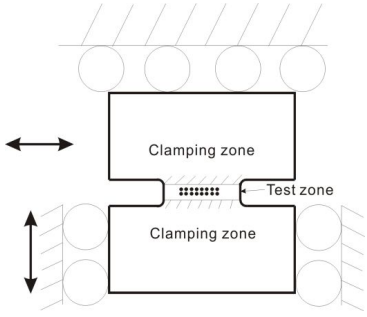

Fig. 3 *Schematic representation of the applied loading*

In the present study, the orthogonal paths tests are conducted on biaxial test equipment developed at the faculty of Engineering Technology at the University of Twente, named TBT tests. The geometry and scheme of the loading method are shown in Fig.2 and Fig.3. Vertical and horizontal actuators are used to deform the specimen. In the critical zone (gage length of 15.0 by 3.0 mm²) optical strain measurement system is used. The overall combined tests were conducted under a constant displacement rate of 1.0 mm/min to ensure the quasi-static conditions and remove the strain rate effect. Via DMC smart Terminal and LabView, the strain of the sample is reflected in the change of the coordinates of the dots (shown in Fig.3) giving an error of the strain measurement less than $5\cdot10^{-4}$ [12].

The finite element model of the specimen is shown in Fig. 4 with 3440 C3D8R solid elements with reduced integration from ABAQUS elements library. The smallest mesh size is 0.3 mm in the gage length of the specimen as shown in Fig. 4.

First, the tension-shear tests are used to determine the distortion parameters X_{l1}^{c}, X_{l1}^{p} and X_{l2}. For tension-shear tests two levels of equivalent plastic strain are reached namely 16.0% and 10.0%. After 16.0% of plastic strain in pre-tensile, the subsequent shear yield stress is 197.0 MPa, while simulated result (without yield surface distortion) gives 220 MPa (Fig. 5). The X_{l1}^{c} value can be fast determined in the plane strain tensile-shear stress space. When X_{l1}^{c} value equal to 30.0, the yield surface can cover the experimental observed yield point $\sqrt{3}\times197$ MPa (shown in Fig. 5). At that time, the kinematic hardening and isotropic hardening value are separately (31.0, -18.0, -18.0, 0.0, 0.0, 0.0) MPa and 49.0 MPa. X_{l1}^{p} controls the flowing trend after yielding, the optimized value was chosen to be 100.0. For the subsequent yield points is not exceed or much lower than the monotonic condition, so the X_{l2} effect can be ignored for AL7020 alloy. Accordingly, with $X_{l1}^{c}=30.0$, $X_{l1}^{p}=100.0$ and $X_{l2}=0.0$, a good fitting is found between experimental and numerically predicted results for pre-strain of 10.0% and 16.0% tensile tests (Fig.6). In Fig. 6(a), the subsequent stress-strain curves are compared with different distortional parameters after 16% plastic strain. It is found that the curve with $X_{l1}^{c}=30.0$, $X_{l1}^{p}=100.0$ is in good agreement with the experimental observed curves. In Fig. 6(b), the comparison between experimental and numerical stress-strain curves after 10% is give.

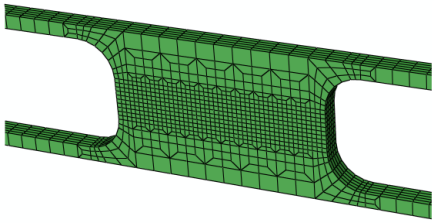

Fig. 4 *Mesh of the specimen*

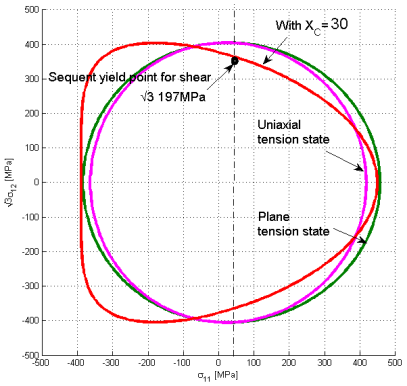

Fig. 5 *Plot of yield surfaces after second pre-tension*

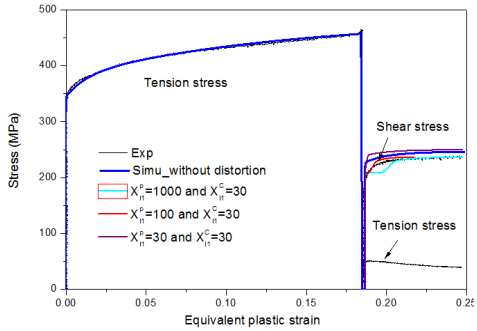

(a)

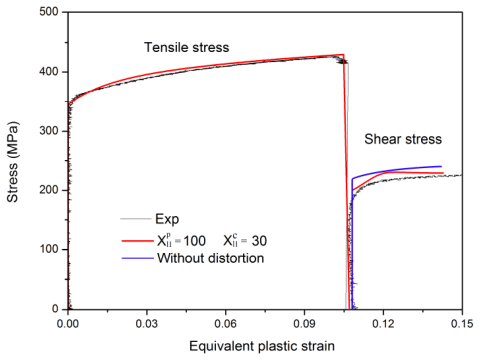

(b)

Fig. 6 *Stress-strain curves after second pre-tension*

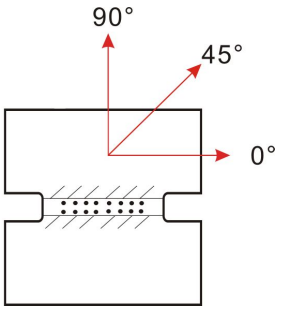

Fig. 7 *Scheme of subsequent loading path*

Concerning the shear-tension tests, the results obtained for three directions 45° and 90° (see Fig. 7) after 10% plastic strain in shear direction are depicted in Fig.8. Clearly, taking into account the distortion effect leads to a better description of the experimental results for both 45° (Fig. 8a) and 90° (Fig. 8b).

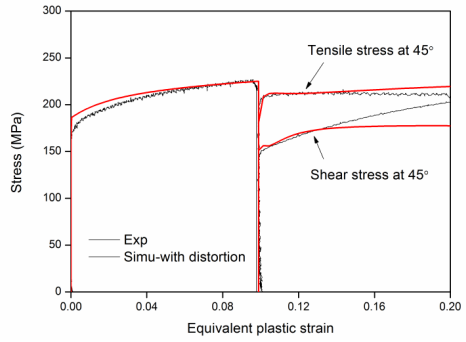

(a)

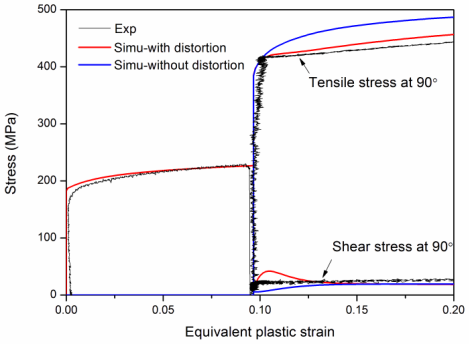

(b)

Fig. 8 *Stress-strain curves after pre-shear in (a) 90° (b) 45°*

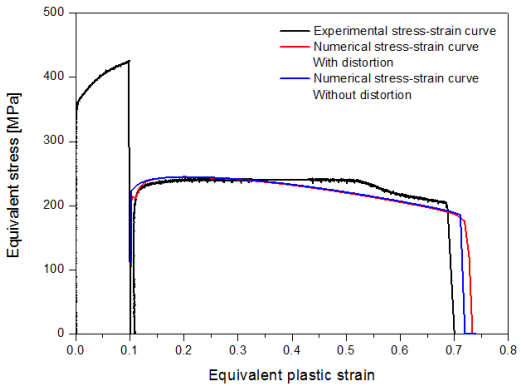

Fig. 9 *Comparison of stress-strain curve until fracture with and without distortion effect*

In Fig. 9, the comparison of the subsquent stress-strain curves until fracture with and without distortion is given. Caused by the decrease of the stress due to the yield surface distortion, the damage potential is reduced that makes the damage evolution slower delaying the time to fracture. Besides, there is still a some deviation between the experimental and numerical stresses for large strains (greater than 40%).

4 Conclusions

In this study, an enhanced fully coupled ductile damage model, developed in a thermodynamically-consistent framework, is proposed. It considers an initial anisotropic yield function and mixed nonlinear kinematic and isotropic hardening. A new developed form of the yield surface distortion approach is given. In order to test the capability of the proposed model, the behavior of sheet metal AL7020 is investigated under simple and complex loading paths. A biaxial loading tester named TWENTE BIAXIAL TESTER is chosen to investigate the subsequent behavior of sheet metal forming.

The Experiment design includes simple loading tests which help determine the elastoplastic and damage parameters covering large range of stress states. Complex or orthogonal loading paths tests which can help determine the parameters X_{l1}^{c} and X_{l1}^{p}. From the simulation results, we can see yield surface distortion help explain the flow stress change in subsequent forming step. The capability of the proposed model is verified by the comparison of stress-strain curves between experimental and numerical results.

REFERENCES

[1] François, M.: *A plasticity model with yield surface distortion for non proportional loading.* International Journal of Plasticity, **17**(5): p. 703-717, 2001.

[2] Hill, R.: *A Theory of the Yielding and Plastic Flow of Anisotropic Metals.* Proceedings of the Royal Society of London. Series A, Mathematical and Physical Sciences, **193**(1033): p. 281-297, 1948.

[3] Hill, R.: *Theoretical plasticity of textured aggregates*. Mathematical Proceedings of the Cambridge Philosophical Society. Vol. 85, Cambridge Philosophical Society 1979.

[4] Hill, R.: *Constitutive modelling of orthotropic plasticity in sheet metals.* Journal of the Mechanics and Physics of Solids, **38**(3): p. 405-417, 1990.

[5] Hosford, W.F.: *A Generalized Isotropic Yield Criterion.* Journal of Applied Mechanics, **39**(2): p. 607-609, 1972.

[6] Yeh, W. and H. Lin: *An endochronic model of yield surface accounting for deformation induced anisotropy.* International Journal of Plasticity, **22**(1): p. 16-38, 2006.

[7] Feigenbaum, H.P. and Y.F. Dafalias: *Directional distortional hardening in metal plasticity within thermodynamics.* International Journal of Solids and Structures, **44**(22-23): p. 7526-7542, 2007.

[8] Barlat, F., J. Ha, J.J. Grácio, M.-G. Lee, E.F. Rauch, and G. Vincze: *Extension of homogeneous anisotropic hardening model to cross-loading with latent effects.* International Journal of Plasticity, **46**: p. 130-142, 2013.

[9] Wu, H.-C. and H.-K. Hong: *Description of yield surface evolution using a convected plasticity model.* International Journal of Solids and Structures, **48**(16-17): p. 2310-2323, 2011.

[10] Feigenbaum, H.P., J. Dugdale, Y.F. Dafalias, K.I. Kourousis, and J. Plesek: *Multiaxial ratcheting with advanced kinematic and directional distortional hardening rules.* International Journal of Solids and Structures, **49**(22): p. 3063-3076, 2012.

[11] Barlat, F., J.J. Gracio, M.-G. Lee, E.F. Rauch, and G. Vincze: *An alternative to kinematic hardening in classical plasticity.* International Journal of Plasticity, **27**(9): p. 1309-1327, 2011.

[12] Riel, M.v. and A.H.v.d. Boogaard: *Measurements and calculations on yield surfaces in tension-simple shear experiments*, in *7th International Conference and Workshop on Numerical Simulation of 3D Sheet Metal Forming Processes, Numisheet 2008*2008: Interlaken, Switzerland. p. 61-66.

[13] Badreddine, H., K. Saanouni, and A. Dogui: *On non-associative anisotropic finite plasticity fully coupled with isotropic ductile damage for metal forming.* International Journal of Plasticity, **26**(11): p. 1541-1575, 2010.

[14] Saanouni, K.: *Damage Mechanics in Metal Forming: Advanced Modeling and Numerical Simulation*. London: ISTE, John Wiley & Sons, 2012.

[15] Yue, Z.M., C. Soyarslan, H. Badreddine, K. Saanouni, and A.E. Tekkaya: *Inverse Identification of CDM Model Parameters for DP1000 Steel Sheets Using a Hybrid Experimental-Numerical Methodology Spanning Various Stress Triaxiality Ratios.* Key Engineering Materials, **554-557**: p. 2103-2110, 2013.

[16] Rousselier, G., F. Barlat, and J.W. Yoon: *A novel approach for anisotropic hardening modeling. Part I: Theory and its application to finite element analysis of deep drawing.* International Journal of Plasticity, **25**(12): p. 2383-2409, 2009.

[17] Yue, Z.M., C. Soyarslan, H. Badreddine, K. Saanouni, and A.E. Tekkaya: *Identification of fully coupled anisotropic plasticity and damage constitutive equations using a hybrid experimental-numerical methodology with various triaxialities.* International Journal of Damage Mechanic, accepted for publication, 2014.